PV SOLAR RADIOMETRIC MEASUREMENTS

Daryl R. Myers, Theodore W. Cannon

National Renewable Energy Laboratory, Golden, CO 80401

Abstract. Radiometric measurements performed by the PV Solar Radiometric Measurements Task support NREL's centers for Measurements and Characterization, Performance Engineering and Reliability, and Renewable Energy Resources. The task provides characterization, measurements, testing, designs, and analysis of radiometric instrumentation and data for the performance of PV cells, modules, and systems. We describe recent characterization of the radiometric performance of pyranometers deployed for PV system testing at the NREL Outdoor Test Facility (OTF) and improvements undertaken in NREL broadband radiometer characterization. Typical measurement and calibration issues with diode array spectroradiometers used for absolute spectral measurements applied to PV performance and characterization are discussed.

PV SYSTEM RADIOMETER EVALUATIONS

Direct-normal or beam radiation and global radiation on plane-of-array (POA) surfaces are typical broadband radiometric measurements for PV performance applications. These devices respond to the total radiation in the spectral region from 280 nm to 2800 nm. Pyrheliometers for measuring the direct beam have uncertainties of 1.5%-2.0% (1,2) and pyranometers for the global (total hemispherical) irradiance with uncertainties of 2%-5% (3).

PV system and module performance testing at NREL relies on well-calibrated individual radiometers assigned to each specific test activity. Each PV system is instrumented with a pyranometer integrated into the system data collection stream. An independent Reference Meteorological and Irradiance System (RMIS), described in previous review meetings(4,5), records 1-minute time-resolved data for quality assurance and special test applications.

In 1996, we evaluated the performance of three of the system radiometers versus the RMIS data under clear, partly cloudy, and overcast conditions for each of the four seasons. Diurnal profiles of RMIS data were examined to identify at least two specific clear, partly cloudy, and overcast days in the spring (March, April, May), summer (June, July, August), fall (September, October, November) and winter (December, January, February)

of 1995. Figure 1 is the RMIS irradiance profile plot for Februrary 5th, 1995, the partly cloudy winter day selected. The plot displays (top to bottom) the 40° tilt, direct-normal, global- horizontal, and diffuse-horizontal irradiances. Table 1 lists the dates selected for this study. The radiometers evaluated were Kipp and Zonen Model CM-11 and CM-21 pyranometers. The pyranometers were installed on the United Solar

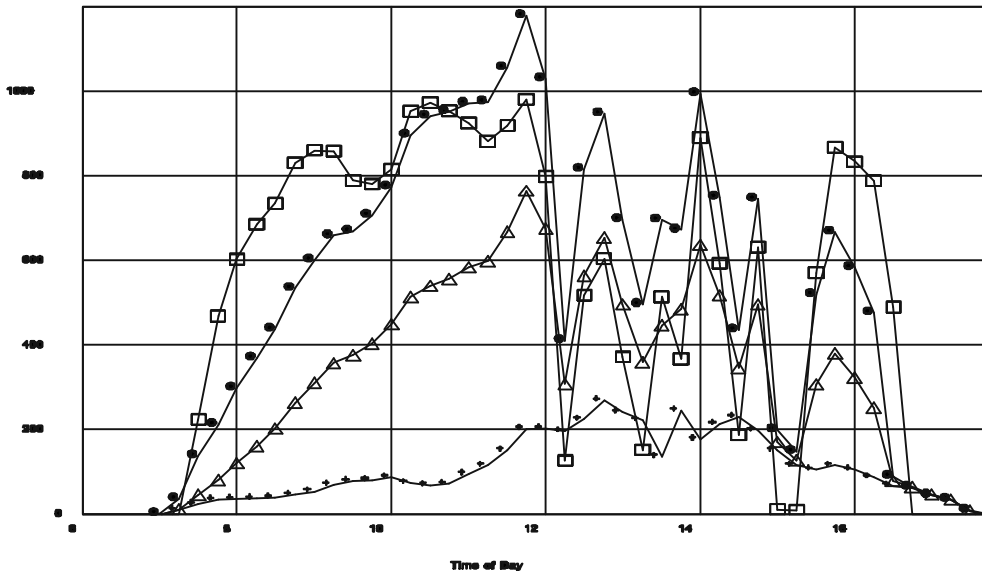

Figure 0. 40° Tilt, direct-beam, global-horizontal, and diffuse-horizontal (top to bottom) profiles for Feb 05, 1995, partly cloudy sky radiometer evaluation.

Table 1. Dates (1995) for Pyranometer Evaluation

SEASON SKY>	Clear	Partly Cloudy	Cloudy
Spring	Mar 14, Apr 01	Apr 30, May 12	Mar 23, May 24
Summer	Jun 18, Aug 01	Jul 24, Aug 12	Jul 30, Jul 31
Fall	Oct 07, Oct 27	Sep 23, Nov 20	Oct 22, Nov 13
Winter	Jan 22, Feb 25	Jan 07, Feb 05	Jan 16, Feb 10

Systems Corporation roofing modules, the Siemens Solar Industries cadmium indium diselenide (CIS) system, and an ASE Americas system(6,7). The radiometers were all installed at 40° (the latitude of the OTF test field is 39.74°N) facing south (azimuth 180° with respect to north=0°). The systems are located along the south edge of the OTF test field, at intervals of about 50 feet from west to east over a distance of about 200 feet. The RMIS station

was located at the northwest corner of the test field, about 100 feet north of the PV system array. RMIS one-minute data were integrated over the 15-minute period used for the three PV system data streams for each of the 24 days of the study. For each fifteen minute period, the average irradiance from the test pyranometers was divided by the RMIS 40°-tilt irradiance. Figures 2 to 4 show the ratios obtained.

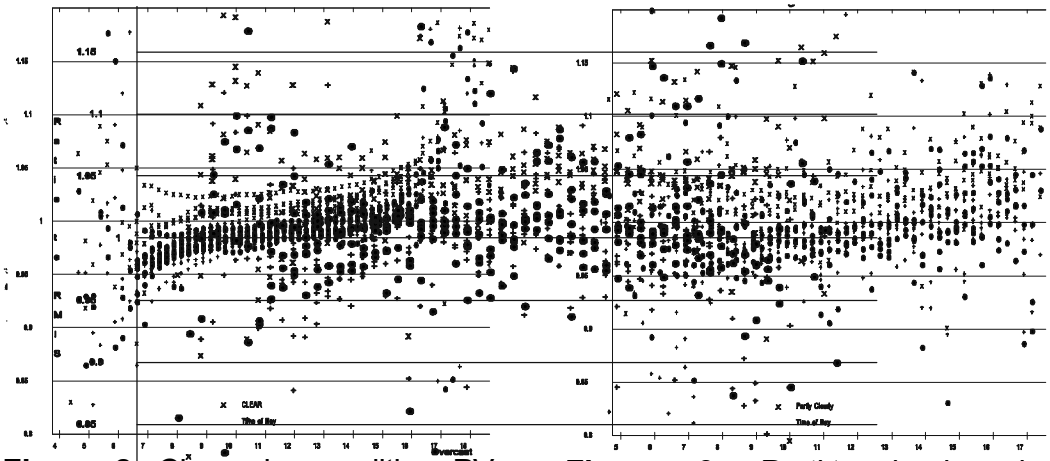

Figure 2. Clear sky condition PV system radiometer ratios to RMIS.

Figure 3. Partly cloudy sky condition PV system radiometer ratios to RMIS.

Figure 4. Overcast sky condition PV system radiometer (+=Roof, o=CIS, x=ASE) ratios to RMIS.

Each plot contains 2 days of ratios for

each of the 3 systems, for all four seasons, or 24 curves. These plots indicate the following:

- For all clear-sky conditions, the four radiometers agreed to within 2.5% from 9 AM until 4 PM.

- Clear-sky range of ratios is within the ±3.0% uncertainties for the instruments when a single calibration responsivity is used.

- Increasing cloudiness results in ratios increasing to ±5% for partly cloudy and ±8% for totally overcast conditions

- The envelope of the ratios increases for all sky conditions in the early morning and late afternoon hours (before 9 AM and after 4 PM).

The increasing ratio envelope with increasing cloudiness is thought to be due to differences in the spatial and temporal distribution of the clouds from each radiometer's point of view (different locations of the instruments), and slight time response differences between the radiometers. Variations in

radiometer temperatures and temperature response may also increase the ratio envelope under cloudier conditions.

The wider envelope in the morning and afternoon ratios is attributed to north-south alignment and geometrical response differences. These are largest for large incidence angles. Figure 5 shows clear-sky data by season for the roofing system radiometer.

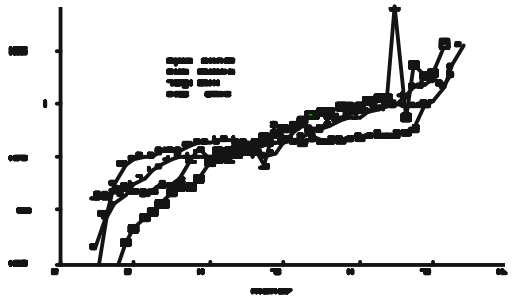

Figure 5. Seasonal variation in ratio of USSC roofing System radiometer to RMIS.

Noontime incidence angles are smallest in the spring and fall, the largest in the winter and summer.

To evaluate the radiometers use in OTF PV testing, we revised our broadband outdoor radiometer calibrations to map incidence angle response in the range from 85° to 0° incidence. We use the same component summation technique (compute the reference irradiance from direct and diffuse data) previously used for horizontal calibrations to radiometers tilted at latitude minus the solar declination for the time period of the outdoor calibration. The diffuse measurement is made with a pyranometer tilted at the same angle with a tracking shading disk to block the direct beam.

This technique achieves normal incident direct beam radiation at solar- noon and responsivity at off-normal incident angles for the rest of the day. We then compute average responsivity within incident angle bins (10 degrees wide) and produce a responsivity versus incident angle plot, with error bars spanning the range of responsivities within a bin.

Figure 6 illustrates the normalized (at 45°) incidence angle response of two different models of pyranometer arrived at using the technique in October of 1996. The unit represented by the open-circle symbols has a much flatter cosine response on average than that of the unit with the cross symbols. The spread of the data within any one range of incidence angles is consistently ±1.0%, representing the random components of uncertainty in the horizontal or this tilted calibration.

This technique maps the instrument response only along the east-west axis of the sensor. We will to investigate the effects of varying the tilt angle to map more completely the cosine response of different regions of the sensor. We do not currently correct our PV system radiometer data for these effects, but hope to apply this calibration technique to all PV system radiometers at the OTF in the coming year.

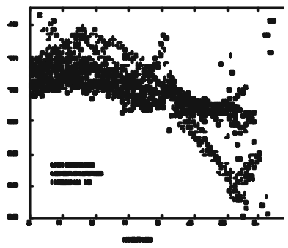

Figure 6. Incidence angle response for two pyranometers at latitude minus declination.

ARRAY SPECTROGRAPH MEASUREMENT ISSUES

Diode array spectroradiometers are relatively inexpensive and readily available from many optical instrumentation manufacturers. These spectro-graphs acquire spectral information in milliseconds that would take minutes to acquire with traditional scanning grating spectro-radiometers as NREL uses and have described elsewhere (4,5,8,9). Using such an instrument, we

became aware of the many difficulties associated in using such a device to measure spectra of pulse solar simulators.

The device used in our study covered the wavelength region from 300 nanometers (nm) to 1100 nm with an array of 1024 diode elements, or an equivalent spectral resolution of about 1 nm. The holographic grating was blazed at 1000 nm. The unit was calibrated for absolute spectral measurements by determining the responsivity (watts per square meter per nanometer)/(digital count) by measuring a 200-watt tungsten halogen lamp with a known spectral distribution. Spectral data were then collected under the NREL Spire 204A pulsed solar simulator. The 240A generates a 3-millisecond (ms) light pulse at 15 Hertz, or a period of 66.67 ms. Figure 7 compares the array radiometer and NREL scanning grating radiometer (Pulse Analysis Spectro-radiometer System, PASS (8)) data, and shows the relative spectral distribution of the calibration lamp in the lower part of the figure.

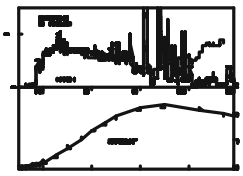

Figure 7. Realtive spectral distribution of Spire 240A measured with diode array and scanning grating spectroradiometers compared with calibration lamp spectrum.

Figure 7 shows that the array radiometer data greatly exceeds the PASS radiometer data greatly in the above 800 nanometers, and is lower than the PASS data in the region from 400 nm to 700 nm. The reasons for these discrepancies are: (1) lack of spectral order sorting filters in the diode array instrument, (2) great disparity in the spectral distributions of the calibration and simulator sources, (3) increased stray light due to the lack of an exit slit in front of the detector(s), and (4) time synchronization between the pulse source and the array data collection.

Gratings used in modern monochromators obey the grating equation, relating the grating spacing (d), the wavelength of impinging radiation (λ), the angle the radiation is incident at (ϕ), and the angle the radiation is diffracted with respect to the normal (θ), and the **order number** (m) where: $d (\sin \phi + \sin \theta) = m \lambda$. The equation indicates that **monochromatic** light will be diffracted in a number of different directions (θ_m for each order multiple m of the wavelength). When broadband light is diffracted from the grating higher orders of shorter wavelength light can overlap the first order of longer-

wavelength light, and contribute to the signal in the longer-wavelength radiation. For example, second order 400-nm radiation will add to the first order 800-nm radiation seen by a detector selecting the 800-nm radiation. This is the primary cause of the excess radiation beyond 800 nm in the array data of Figure 7. The second-order radiation from the high irradiance levels at 400 nm to 800 nm overlap the first order radiation in the 800 nm to 1000 nm region, contributing a significant error to the signal beyond 800 nm.

Selection of an order-sorting (cut-on) filter to pass radiation of wavelength greater than about 600 nm and to reject radiation below that wavelength would allow only first-order 600-nm to 1100-nm light to reach the detector and produce a more accurate spectrum. This complicates the calibration and use of the array radiometer. At least two array spectral measurements are required, because the low wavelength data would have to be acquired without the filter in place and the longer wavlength data with the filter in place. This requires a calibration for the array radiometer with and without the filter in place and a combination of the two measured spectra to produce the final composite spectrum. Some array detectors are available with integral order-sorting filters deposited on the elements for detecting longer wavelengths.

The significantly different shapes of the calibration and measurement spectra, in conjunction with the problem of order sorting further complicates the interpretation of the measured data. There is relatively low energy in the 300 nm to 600 nm region of the standard lamp spectrum. The contribution of the higher orders of shortwave radiation to the first-order longer-wave radiation is much different than in the pulse simulator xenon source case. The calibration without the use of order sorting carries appropriate information only for sources with similar relative spectral distributions and not for any other unknown spectral distribution to be measured.

In addition to the above concerns, an understanding of the operation of this particular array radiometer is essential to obtaining meaningful data. A very simplified outline of the operation of the radiometer follows to illustrate the point.

The array used in the spectrograph is continually accumulating charge as long as the instrument is running. An operational cycle is carried out continuously by the instrument. The cycle consists of accumulating charge for a "Blanking time" of at least 6.84 ms, then "reading" the array by reading out (discharging) the array (so it does not eventually saturate) during the next 13.16 ms. The "blanking" time, or time of data acquisition can be extended by the user. When light reaches the detector array, charge builds up in each array element over the 6.84 blank time, and it is read out and processed during the 13.16-ms read time. Figure 8 is a diagram of this process compared to the duty cycle of a typical pulse simulator.

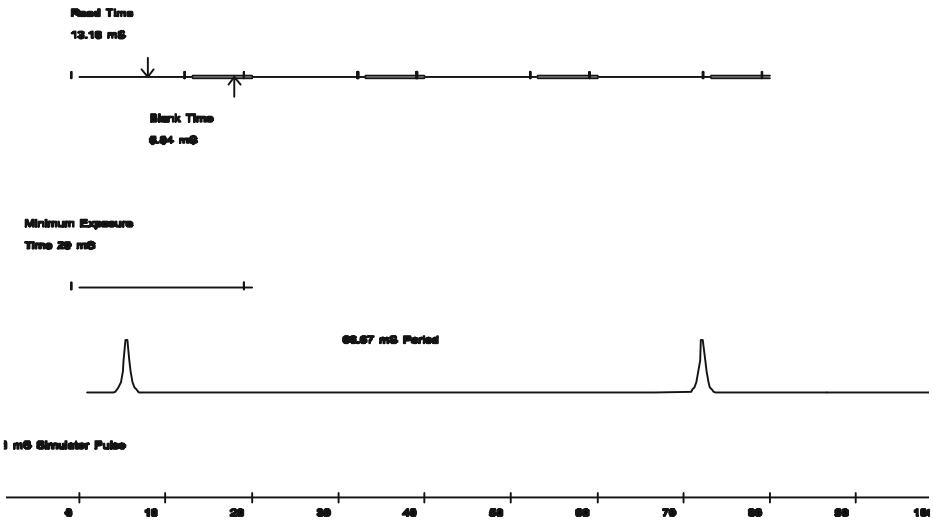

Figure 8. Timing diagram for array spectroradiometer data collection.

During calibration, the standard source is on continuously, so charge accumulates during each (minimum) 6.84-ms blanking interval. During the measurement of a 3-ms pulse from the Spire 240A, charge only builds up over the short 3-ms period, which may or may not occur totally within the blanking interval. The temporal duration of the charge build-up must be accounted for in the two different situations to get easily interpreted measured spectra. The array essentially produces a signal proportional to the *energy* seen during the blanking period. Without knowledge of the pulse shape and appropriate time synchronization between the pulse and the opertional cycle of the array radiometer, only a portion, or none, of a pulse may be captured.

CONCLUSION

The interpretation of PV module and system performance characterization at NREL requires accurate radiometric measurements. We intend to apply a modified component summation technique for outdoor broadband radiometer calibrations to map out and correct for geometrical response deviations in the pyranometers deployed at the NREL OTF test site. By calibrating radiometers (that are insensitive to tilt) tilted at latitude minus the solar declination, their response over a range of incidence angles from 0° to at least 85° can be obtained.

The advent of diode array spectrographic instruments provides the opportunity to acquire spectral data very quickly and in great quantity. However, even the makers of these instruments state that use of the

instruments for absolute spectral radiometric measurements is "notoriously difficult". An understanding of the operational character-istics of such instrumentation, as well as the attention to the classical principles of diffraction grating dispersion is required to obtain data that is not confusing or, at best, difficult to interpret. The NREL PV Solar Radiometric
Measurements task is working with instrument manufacturers and PV industry and research and development users to achieve useful diode array spectral data.

ACKNOWLEDGEMENTS

Troy Strand, Kieth Emery, Benjamin Kroposki, Steven Rummel, and Robert Hansen helped greatly with data collection at the Outdoor Test Site. Steve Hogan of Spire Corporation loaned the array spectrogaph for testing. Richard DeBlasio, project leader, and Roland Hulstrom, Director for the Center for Performance and Reliability Engineering, provided helpful project guidance. This work was supported by U.S. Department of Energy contract No. DE-AC36-83CH10093.

REFERENCES

1. Myers, D. R., Stoffel, T.L., "A Description of the Solar Radiometer Calibration (RADCAL) Process at SERI." *Proceedings of 1990 Annual Conference of the American Solar Energy Society*. *Austin, TX. March 19-22, 1990*. p. 171.

2. Myers, D. R., "Application of a Standard Method of Uncertainty Analysis to Solar Radiometer Calibrations." *Proceedings of 1989 Annual Conference of The American Solar Energy Society. Denver, CO. Jun 19-22, 1989.* p. 445.

3. Myers, D. R., Emery,K., Stoffel,T.L., "Uncertainty Estimates for Global Solar Irradiance Measurements Used to Evaluate PV Device Performance," *Solar Cells*, 27, 1989. p. 456.

4. Myers, D.R., Cannon, T., "Photovoltaic Radiometric Measurements and Evalutation", *13th NREL Photovoltaics Program Review, AIP Conference Proceedings 353*. American Institute of Physics, Woodbury, NY, 1995. p. 177.

5. Myers, D.R., and T. Cannon, "Technical Overview of Solar Radiation Research at NREL", *12th NREL Photovoltaics Program Review, AIP Conference Proceedings 306*. American Institute of Physics, Woodbury, NY, 1993. p. 137.

6. Mrig, L., Caiyem, Y., Rummel, S., Hansen, R., Kroposki, R., Strand, T., "Photovoltaic Module and System Performance Testing at NREL",*12th NREL Photovoltaics Program Review, AIP Conference Proceedings 306*. American Institute of Physics, Woodbury, NY, 1993. p. 164.

7. Mrig, L., Hansen, R.,Kroposki, B., Strand, T.,"Results of Module and System Testing at NREL", *13th NREL Photovoltaics Program Review, AIP Conference Proceedings 353*. American Institute of Physics, Woodbury, NY, 1995. p. 207.

8. Myers, D.R., Cannon, T., Trudell, D., "Radiometric Measurements for PV Characterization", *Proceedings of the PV Performance and Reliability Workshop, Sept. 8-10*, *1993*. National Renewable Energy Laboratory, Golden Co. 80401.

9. Cannon, T. W., Hulstrom, R.L., Trudell, D.T., "New Instrumentation for Measuring Spectral Effects During Indoor and Outdoor PV Device Testing", *The Conference Record of the Twenty Third IEEE Photovoltaic Specialists Conference-1993, Louisville, KY. May 1993*, P. 1176.